**NASA TECHNICAL NOTE**

NASA TN D-6676
c.1

NASA TN D-6676

# ON THE STABILITY AND POINTING OF AN ATTACHED DOUBLE-GIMBAL EXPERIMENT PACKAGE

*by Nelson J. Groom, John D. Shaughnessy, and Vilas D. Nene*

*Langley Research Center*
*Hampton, Va. 23365*

| 1. Report No. NASA TN D-6676 | 2. Government Accession No. | 3. Recipient's Catalog No. |
|---|---|---|
| 4. Title and Subtitle ON THE STABILITY AND POINTING OF AN ATTACHED DOUBLE-GIMBAL EXPERIMENT PACKAGE | | 5. Report Date April 1972 |
| | | 6. Performing Organization Code |
| 7. Author(s) Nelson J. Groom, John D. Shaughnessy, and Vilas D. Nene* | | 8. Performing Organization Report No. L-7898 |
| | | 10. Work Unit No. 115-19-02-03 |
| 9. Performing Organization Name and Address . NASA Langley Research Center Hampton, Va. 23365 | | 11. Contract or Grant No. |
| | | 13. Type of Report and Period Covered Technical Note |
| 12. Sponsoring Agency Name and Address National Aeronautics and Space Administration Washington, D.C. 20546 | | 14. Sponsoring Agency Code |

15. Supplementary Notes

With appendix A by William C. Walton, Jr., of the Langley Research Center.

*NRC-NASA Resident Research Associate at NASA Langley Research Center.

16. Abstract

The pointing capability of a double-gimbal experiment isolation and control system of the Apollo Telescope Mount (ATM) type is investigated. Three composite structural models of an experiment package connected through frictionless gimbals to a carrier vehicle (including a rigid-package—rigid-carrier model, a rigid-package—flexible-carrier model, and a flexible-package—flexible-carrier model) are used for this investigation, and a linear model of the nominal ATM gimbal control system is considered. Contributions of the primary carrier control system to experiment pointing are neglected. A linear stability analysis is performed to verify stability of the experiment control system with nominal gains. Transform techniques are then used to compute pointing errors onboard the experiment package due to random crew motions input into the carrier vehicle. Results of the investigation indicate that there is no stability problem due to flexible coupling of the experiment package and the carrier, and that the ATM-type double-gimbal experiment isolation and control system is capable of pointing accuracies better than 0.1 arc second.

| 17. Key Words (Suggested by Author(s)) Experiment package Stability and control Experiment isolation and control | 18. Distribution Statement Unclassified — Unlimited | | |
|---|---|---|---|
| 19. Security Classif. (of this report) Unclassified | 20. Security Classif. (of this page) Unclassified | 21. No. of Pages 43 | 22. Price* $3.00 |

# ON THE STABILITY AND POINTING OF AN ATTACHED
# DOUBLE-GIMBAL EXPERIMENT PACKAGE

By Nelson J. Groom, John D. Shaughnessy,
and Vilas D. Nene*
Langley Research Center

## SUMMARY

The pointing capability of a double-gimbal experiment isolation and control system of the Apollo Telescope Mount (ATM) type is investigated. Three composite structural models of an experiment package connected through frictionless gimbals to a carrier vehicle (including a rigid-package—rigid-carrier model, a rigid-package—flexible-carrier model, and a flexible-package—flexible-carrier model) are used for this investigation, and a linear model of the nominal ATM gimbal control system is considered. Contributions of the primary carrier control system to experiment pointing are neglected. A linear stability analysis is performed to verify stability of the experiment control system with nominal gains. Transform techniques are then used to compute pointing errors onboard the experiment package due to random crew motions input into the carrier vehicle. Results of the investigation indicate that there is no stability problem due to flexible coupling of the experiment package and the carrier, and that the ATM-type double-gimbal experiment isolation and control system is capable of pointing accuracies better than 0.1 arc second.

## INTRODUCTION

By placing telescopes in orbit above the atmosphere, several severe limitations that have hampered ground-based astronomy are removed (opacity of the atmosphere in certain wavelength regions and scattering of light from scattering centers), and by having the telescope station manned, maximum information can be obtained (ref. 1). In order to achieve the necessary pointing accuracy for astronomy experiments on a manned vehicle, however, some method of isolating the experiments from crew-motion-induced disturbances is usually necessary. One method of isolation and control is to attach the experiment package to the main vehicle through two gimbals with the center of mass of the package being placed as close as possible to the intersection of the gimbal axes. The

---

package is then controlled with respect to the main vehicle by gimbal torquers. This method will be implemented with the Apollo Telescope Mount (ATM), which will be one of the experiments on the Skylab mission (ref. 2). The ATM houses solar astronomy experiments and has a specified pointing accuracy of 2.5 arc seconds (defined here as the accuracy of maintaining a certain acquired attitude as opposed to the accuracy of acquiring the attitude). An ATM-type system is also being considered for use with advanced stellar telescopes which require a pointing accuracy of 0.1 arc second.

The ATM double-gimbal concept has two inherent sources of error which limit the pointing accuracy that can be achieved. One of these sources results from the fact that the center of mass of the experiment package cannot be placed exactly at the intersection of the gimbal axes. Consequently, translational acceleration and rotational motion about the pointing axis of the package produces an inertia torque which acts as a disturbance. The other source is due to the design itself; since there are only two degrees of freedom (rotation about the gimbal axes), the system provides essentially no isolation from translational inputs. Thus, disturbance in the carrier vehicle could cause the experiment package to be subjected to considerable vibration. If the experiment package were perfectly rigid, then the center-of-mass offset would be the only source of error. The experiment package, of course, is not perfectly rigid, so bending of the experiment package due to translational and rotational motion (about the pointing axis) of the gimbal attachment points must be considered as a source of error.

The ATM-type system has been investigated for a nonplanar flexible carrier and rigid experiment package with nonlinear control (ref. 3), and a flexible model of the experiment package has been analyzed by using a planar model attached to a rigid support with linear control (in an investigation conducted by the Space Support Division of Sperry Rand Corporation under contract to George C. Marshall Space Flight Center). The present investigation considers the pointing accuracy of a linear model of the ATM-type system for three nonplanar composite structural models ((1) a rigid-package—rigid-carrier model, (2) a rigid-package—flexible-carrier model, and (3) a flexible-package—flexible-carrier model) to determine what effect the basic design limitations of the ATM-type system might have on achieving a pointing accuracy of 0.1 arc second in the presence of random crew motions at various points in the carrier vehicle. These three models were examined to determine, respectively, (1) the effects of package center-of-mass offset, (2) the combined effects of package center-of-mass offset and carrier flexibility, and (3) the combined effects of package center-of-mass offset, package flexibility, and carrier flexibility.

The method of computing the vibration modes of the coupled carrier—experiment-package structure is described in appendix A by William C. Walton, Jr., of the Langley Research Center.

Crew motions are represented by a filtered random number sequence (with Gaussian distribution and negligible mean) which describes continuous motion of a single astronaut performing different tasks. Pointing errors were computed by using transform techniques. Errors were computed on a 3-sigma basis at the fine sun sensor and each experiment location in pitch and yaw. Only pitch and yaw were used since the experiment control system exerts no active control in roll.

## SYMBOLS

[A]  coefficient matrix

$\{B\} = [A]\{\hat{T}\}$

[CONN]  matrix defining the connection between carrier and telescope

[CUP]  coupling matrix for carrier and telescope modes

$\{d\}$  translations and rotations for coupled system

$\{D\}$  Laplace transform of $\{d\}$

$\{DC\}$, $\lfloor DC \rfloor$  deformation vectors used in calculation of carrier modes

$\{DT\}$, $\lfloor DT \rfloor$  deformation vectors used in calculation of telescope modes

$\{DRAPC\}$  deflection-rotation vector for telescope attachment point in carrier coordinates

$\{DRAPT\}$  deflection-rotation vector for telescope attachment point in telescope coordinates

e  base of natural system of logarithms, 2.71828

$\{E\}$  vector of total generalized force for coupled system

[ECC]  telescope mass-point coordinate matrix

$\{EDT\}$, $\lfloor EDT \rfloor$  elastic deformation vectors used in calculation of telescope modes

$\{\bar{E}\}$        Laplace transform of  $\{E\}$

$f$          frequency variable

$f(t)$        input to system, a continuous function of time

$f(k)$       an array obtained by sampling function  $f(t)$

$f_f$        folding frequency

$f_0$        fundamental frequency

$f_s$        sampling frequency

$F(j)$       discrete Fourier transform of  $f(k)$

$F(\omega)$      continuous Fourier transform of  $f(t)$

$\bar{F}(s)$       Laplace transform of input to crew-motion filters

$\lceil GMC \rfloor$    diagonal matrix of generalized carrier masses

$\lceil GMT \rfloor$    diagonal matrix of generalized telescope masses

$h(t)$        impulse response of system, a continuous function of time

$H_1, H_2$     transfer function blocks in system feedback loop

$H_s$         fine-sun-sensor gain

$H(\omega)$      continuous Fourier transform of  $h(t)$

$\bar{H}(s)$       generalized transfer function in  $s$  domain

$i = \sqrt{-1}$

$[I]$         identity matrix

Im         imaginary part of

4

j,k,m,n        integers

K             represents a given transfer function block in system forward loop (with subscripts 1 to 12)

$K_a K_m$       torque-motor gain

$K_{rg}$        rate-gyro gain

[KC]       symmetric stiffness matrix used to compute carrier modes

[KT]       symmetric stiffness matrix used to compute telescope modes

L             Lagrangian

$$\left\lceil M \right\rfloor = [I]s^2 + 2(0.01)\left\lceil \omega_n \right\rfloor s + \left\lceil \omega_n^2 \right\rfloor$$

[MC]      symmetric mass matrix used to compute carrier modes

$\left[ \overline{MC} \right]$      carrier mass matrix [MC] with telescope mass deleted

[MT]       symmetric mass matrix used to compute telescope modes

N            number of points in sequences f(k), r(m), and so forth

{q}        vector of modal deflections for coupled system

{Q}        Laplace transform of {q}

{QC}, ⌊QC⌋   vectors of carrier mode coordinates

{QT}, ⌊QT⌋   vectors of telescope mode coordinates

r(m)        an array obtained by sampling function r(t)

r(t)         output of system, a continuous function of time

R(m)       discrete Fourier transform of r(m)

| | |
|---|---|
| $R(\omega)$ | continuous Fourier transform of $r(t)$ |
| $\bar{R}(s)$ | Laplace transform of linear-system output |
| Re | real part of |
| s | Laplace operator |
| t | time variable |
| T | periodicity of $f(t)$, if $f(t)$ is periodic, or period of interest |
| $\{\hat{T}\}$ | transfer functions obtained by dividing given $\epsilon$ by given input |
| $[TAP]$ | $6 \times 6$ telescope-attachment-point transformation matrix |
| $[U]$ | modal matrix for coupled system |
| $[UD]$ | modal participation matrix for coupled system |
| $[UF]$ | modal distribution matrix for coupled system |
| $\{U\dot{Q}C\}$ | carrier mode shapes (eigenvectors) for coupled system |
| $\{UQT\}$ | telescope mode shapes (eigenvectors) for coupled system |
| $[UQC], [UQT]$ | matrices of eigenvectors |
| $[UC]$ | matrix of carrier modes |
| $[UT]$ | matrix of telescope modes |
| $\lceil WSQC \rfloor$ | diagonal matrix of squares of carrier-mode natural frequencies |
| $\lceil WSQT \rfloor$ | diagonal matrix of squares of telescope-mode natural frequencies |
| $X_C, Y_C, Z_C$ | carrier axes |
| $X_T, Y_T, Z_T$ | telescope axes |

6

$\Delta f$        sampling interval in frequency domain

$\Delta t$        sampling interval in time domain

$\epsilon$        error point in block diagram representation of system (with subscripts 1 to 20)

$\theta_{cy}$        command input to $Y_T$-axis fine sun sensor

$\theta_{cz}$        command input to $Z_T$-axis fine sun sensor

$\theta_{ey}$        pointing error at fine-sun-sensor location about $Y_T$-axis

$\theta_{ez}$        pointing error at fine-sun-sensor location about $Z_T$-axis

$\rho_g$        rate-gyro damping ratio

$\rho_1, \rho_2$        damping ratios in crew-motion filter equations

$\sigma$        standard deviation

$\tau_a$        torque-motor time constant

$\tau_s$        fine-sun-sensor time constant

$\tau_1, \tau_2$        time constants in crew-motion filter equations

$\omega$        frequency variable

$\bar{\omega}_1, \bar{\omega}_2$        natural frequencies in crew-motion filter equations

$\omega_f$        folding frequency

$\omega_g$        rate-gyro natural frequency

$\omega_n$        natural frequencies for coupled-system vibration modes

Notation:

[ ]          rectangular matrix

$[\ ]^T$         transpose of  [ ]

$[\ ]^{-1}$        inverse of  [ ]

$\left[-\!\!+\!\!-\right]$         partitioned matrix

$\left[\begin{smallmatrix}\ \end{smallmatrix}\right]$         diagonal matrix

{ }          column vector

⌊ ⌋          row vector

$\left\{--\right\},\left\lfloor\ \vdots\ \right\rfloor$ partitioned vectors

    A single dot over a symbol denotes a first derivative with respect to time.  Double dots denote a second derivative.

### ABBREVIATIONS

AM          airlock module

ATM          Apollo Telescope Mount

CFT          continuous Fourier transform

CMG          control-moment gyroscope

CSM          command and service module

c.m.          center of mass

DFT          discrete Fourier transform

FFT          fast Fourier transform

LM          lunar module

MDA         multiple docking adapter

OWS         orbital workshop

## DESCRIPTION OF STRUCTURAL MODELS

There are three structural models used in this paper. Each represents a mathematical model of the ATM experiment package connected through frictionless gimbals to a preliminary version of the Skylab space station.

One model, henceforth called the flexible-body model, consists of a flexible ATM package connected to a flexible model of the Skylab carrier vehicle. The mathematical model was formulated from independent structural models for the Skylab and ATM spar canister by using the method given in appendix A. The independent structural models were developed under separate contracts to George C. Marshall Space Flight Center. The resulting composite model consisted of 107 flexible-body modes, with frequencies ranging from 0.135 Hz to 38.443 Hz, and eight rigid-body modes (six for the Skylab and two for the ATM package).

The second model, henceforth called the rigid-ATM model, consists of a rigid ATM package connected to a flexible model of the Skylab carrier vehicle. This model was developed by using the data from the flexible-body formulation except that the flexible ATM package modes were omitted. The resulting composite model had 93 flexible-body modes, with frequencies ranging from 0.135 Hz to 22.777 Hz, and the same eight rigid-body modes as in the model just described.

A third model, henceforth called the rigid-body model, represents a rigid ATM package connected to a rigid model of the Skylab carrier vehicle. This mathematical model was obtained by dropping all the flexible-body modes. The resulting composite model had the same eight rigid-body modes as in the other two models.

The Skylab configuration considered, shown in figure 1, is composed of a Saturn IV-B orbital workshop (OWS), a multiple docking adapter (MDA), a command and service module (CSM), and a modified lunar module (LM) with a rack which provides attachment points for solar panels, control-moment-gyroscope (CMG) hardware, and the ATM gimbal suspension system.

The example ATM configuration shown in figure 2 is composed of a double-gimbal suspension system with frictionless zero stiffness bearings, an outer shell canister, and a cruciform spar to which eight solar astronomy experiments, four rate-gyro packages,

one two-axis sun sensor, and other equipment are attached. At each gimbal point, a direct-current (dc) torquer is used to provide control torques for the ATM package.

The mathematical representation of the structural models is based on the assumption usually made (see refs. 3 and 4, for example) that structural damping, which is not included in the modal analysis, can be added in an uncoupled sense in modal coordinates. A value of 1 percent of critical damping is assumed to act on each flexible mode. The use of this value is consistent with previous analyses (for example, refs. 3 and 5). This formulation results in the equations of motion given as

$$\{\ddot{q}\} + 2(0.01)\left\lceil \omega_n \right\rfloor \{\dot{q}\} + \left\lceil \omega_n{}^2 \right\rfloor \{q\} = [UF]^T\{E\} \tag{1}$$

Here, $\{q\}$ is the 115-component vector of modal displacements, $\left\lceil \omega_n \right\rfloor$ is the diagonal matrix of modal frequencies, and $[UF]^T$ is the matrix of modal data that distributes the force vector $\{E\}$ over the 115 modes and is found by transposing the matrix $[UF]$ formed from the modal matrix of the coupled carrier-experiment system $[U]$ (see eq. (A13)) by retaining only those rows corresponding to force or torque application locations and directions. The resulting motion in carrier coordinates is given by the relation

$$\{d\} = [UD]\{q\} \tag{2}$$

where $[UD]$ is the matrix formed from $[U]$ by retaining those rows that correspond to the motion of the mass point of interest.

## DESCRIPTION OF CONTROL SYSTEM

The experiment control system used in this paper is a linear model of the ATM system with the roll control system fixed (the roll system is manually controlled prior to experiment initiation). The system consists of a two-degree-of-freedom vernier gimbal system driven by two dc torque motors per axis with error signals derived from a two-axis fine sun sensor and rate gyros mounted on the experiment package. A block diagram of the system used is presented in figure 3, and table I gives the parameters used.

Since the CMG system, which provides Skylab spacecraft stabilization, is designed to control rigid-body motion resulting from low-frequency, low-magnitude torques instead of crew-motion disturbances (ref. 3), no primary CMG control system was included.

# CREW-MOTION MODEL

Previously, deterministic approximations of typical astronaut movements were employed to represent crew-motion disturbances (see appendix II of ref. 6). Recent studies have developed linear filters that can be used in conjunction with a unity-power-spectral-density noise source with Gaussian distribution and negligible mean to represent complete activities such as the performance of a given experiment. These activities combine most of the typical astronaut movements described in reference 6.

The crew-motion input disturbances for this paper were obtained by passing a computer-generated pseudo-random number sequence with a unity power spectral density and Gaussian distribution with negligible mean through appropriate linear filters. Three separate activities were chosen as being representative. These activities consisted of two manual console operations and one compressive walking activity. All three are modeled as single-astronaut motion. The resultant filters have a general transfer function $\overline{H}(s)$ given by

$$\overline{H}(s) = \frac{\tau_1 s \left( \tau_2 s + 1 \right)}{\left( s^2 + 2\rho_1 \overline{\omega}_1 s + \overline{\omega}_1^2 \right) \left( s^2 + 2\rho_2 \overline{\omega}_2 s + \overline{\omega}_2^2 \right)} \tag{3}$$

The values of the parameters in equation (3) are given in table II for each crew activity. The two manual console operations are restrained activities. That is, the astronaut is restrained (by harnesses or other restraining devices) from large translational movements of his center of mass. These two activities (Run 1 and Run 4) represent an astronaut performing the S 056 and S 082A ATM experiments (these experiments are defined in ref. 1). The compressive walking activity is an unrestrained activity which consists of lateral translation between structures where the astronaut can support himself with hands and feet simultaneously. The filters and parameters were developed by Martin Marietta Corporation under contract to George C. Marshall Space Flight Center. The method used to develop the filter transfer functions is given in reference 7. The crew motions were input into two different locations in the carrier vehicle: the AM/MDA intersection and the OWS crew location (fig. 1). All three activities were investigated for the first location, whereas only compressive walking was assumed for the OWS crew location.

# METHOD OF ANALYSIS

The experiment-package pointing errors were computed by convolving the transfer function between the input to the crew-motion filters and the fine-sun-sensor outputs

$\left(\overline{F}(s)/\epsilon_6 \quad \text{and} \quad \overline{F}(s)/\epsilon_{12} \quad \text{in fig. 3}\right)$ with a random number sequence. The random number sequence had a unity power spectral density and a Gaussian amplitude distribution with negligible mean. The frequency-domain transfer-function equations are developed in appendix B. The convolution was performed by using discrete Fourier transform (DFT) techniques and consisted of (1) computing the numerical value of the transfer function of interest at discrete values of $j\omega$, (2) taking the forward DFT of the random number sequence representing the input, (3) multiplying point by point the sequence representing the numerical value of the transfer function and the DFT of the input, and (4) taking the inverse DFT of the product to obtain a sequence representing the error time history of interest. The analytical details of this method are given in appendix C. Table III gives the parameters used in the actual computation of error time histories. The $3\sigma$ values of pointing errors were computed from these time histories. All forward and inverse transforms were computed by the fast Fourier transform (FFT) algorithm which is sometimes called the Cooley-Tukey algorithm (ref. 8). All computations were performed on a Control Data 6600 computer system.

## RESULTS AND DISCUSSION

### Stability

A linear stability analysis was performed to verify that the control system being considered was stable with the nominal ATM torque-motor gain $\left(2K_aK_m\right)$. The stability analysis was conducted by applying the Nyquist stability criterion to the open-loop transfer function of each loop $\left(\theta_{cy}/\epsilon_6 \quad \text{and} \quad \theta_{cz}/\epsilon_{12} \quad \text{in fig. 3}\right)$ with the other loop closed. The upper limit of $2K_aK_m$ for stability was found to be 136.9 N-m/volt. It was expected that including the flexible model of the carrier in the stability analysis instead of assuming a rigid immovable base would result in a stable gain much lower than the nominal, especially since the nominal ATM control loop contains no compensation. However, as the results show, stability is not a problem for the model analyzed and the nominal gain could, in fact, be increased.

### Rigid-Body Model

Results obtained by subjecting the rigid-body model to crew-motion disturbances are presented in table IV. Since the total angular errors at different points of the experiment package are the same for the rigid-body case, only the fine-sun-sensor errors are given. These results represent errors due entirely to the center-of-mass offset since no flexibility is involved. The center-of-mass offset for the experiment-package model (in experiment-package coordinates) was computed from the ATM mass data as (-0.000914, 0.02275, -0.02159) in meters. This amount of offset can be considered to be

excessive since it is possible to reduce the offset to 0.00127 meter along each axis by careful balancing (ref. 3).

## Rigid-ATM Model

Results obtained by subjecting the rigid-ATM model to crew-motion disturbances are presented in table V. Again, only the fine-sun-sensor errors are given because the experiment package is rigid. These results represent combined effects of experiment-package center-of-mass offset and carrier-vehicle flexibility. In some cases, the addition of the carrier flexibility caused an increase in the $3\sigma$ pointing error of almost an order of magnitude. The maximum error, however, was still well below 0.1 arc second.

## Flexible-Body Model

Results obtained by subjecting the flexible-body model to crew-motion disturbances are presented in table VI. Again, only the fine-sun-sensor errors are given because it was found that, although the total angular errors at different points of the experiment package were not exactly equal, the differences were insignificant. These results represent errors due to the combined effects of experiment-package center-of-mass offset, experiment-package flexibility, and carrier-vehicle flexibility. In some cases, the experiment-package flexibility caused an increase in the $3\sigma$ pointing error by a factor of approximately 3 over the rigid-ATM-model errors. Thus, not only bending of the carrier but also bending of the experiment package appears to be a significant contributor to pointing error. Also, since the maximum $3\sigma$ error was approximately 0.02 arc second, the basic design limitations of the ATM-type system appear to present no obstacle in achieving a pointing accuracy of 0.1 arc second.

## Multiple Crew Motion

The errors for each structural model are computed for single-astronaut motion. Since there will be more than one crew member, it is likely that there will be more than one astronaut disturbance at any given time. Since the systems analyzed are linear systems, a worst-case estimate of errors due to multiple crew motion can be made by simply adding $3\sigma$ errors for different single-astronaut disturbances.

## Gain Sensitivity

In order to determine the sensitivity of the gimbal control loops to changes in gain, runs with different gains were made by using one carrier location and one crew-motion input. The carrier location was the AM/MDA intersection and the crew motion was Console Operation Run 1. A plot of $3\sigma$ error as a function of gain is shown in figure 4 for the fine-sun-sensor $Y_T$-axis and the fine-sun-sensor $Z_T$-axis. The sensitivity of the

pointing error of the basic ATM-type gimbal control loop to changes in torque-motor gain suggests that the application of optimal control concepts could result in a significant reduction of overall pointing error.

## CONCLUDING REMARKS

In order to examine the inherent design limitations of a double-gimbal experiment isolation and control system of the Apollo Telescope Mount (ATM) type, three mathematical structural models of an experiment package (ATM) connected through frictionless gimbals to a flexible carrier vehicle (Skylab) were utilized. The three models consisted of the following:

(1) The rigid-body model of the experiment package connected to the rigid-body model of the carrier vehicle

(2) The rigid-body model of the experiment package connected to the flexible model of the carrier vehicle

(3) The flexible model of the experiment package connected to the flexible model of the carrier vehicle

A linear model of the nominal ATM gimbal control system with no sensor, actuator, or bearing nonlinearities was used, and no control-moment-gyroscope control system for the carrier vehicle was included. The stability of the ATM gimbal control system was investigated on the model of the flexible experiment package connected to the flexible carrier vehicle since, on this model, the actuators would be torquing against a flexible structure instead of a fixed rigid base as is normally assumed. The models were subjected to continuous single-astronaut crew motion, represented by a filtered random number sequence with Gaussian distribution and negligible mean, and pointing errors were computed on a 3-sigma basis about the two gimbal axes of the experiment package at the fine-sun-sensor location.

The results of analyses performed on the composite models indicate the following:

1. No stability problem is expected to result from flexible coupling of the experiment package and carrier vehicle.

2. There is enough coupling between flexible-experiment-package modes and flexible-carrier modes that bending of the experiment package must be considered a significant contributor to experiment-package pointing error.

3. The ATM double-gimbal experiment isolation and control system design is inherently capable of providing pointing accuracy better than 0.1 arc second.

4. The application of optimal control concepts to the basic ATM-type gimbal control loop could result in a significant reduction of overall pointing error.

In practice, sensor, actuator, and bearing anomalies, which were neglected for this study, could be limiting factors as far as achieving 0.1-arc-second pointing accuracy in the presence of crew disturbances. A nonlinear study of the double-gimbal system, utilizing the composite models developed in this report, would be required to determine what effect these anomalies would have.

Langley Research Center,
National Aeronautics and Space Administration,
Hampton, Va., February 24, 1972.

# APPENDIX A

## METHOD FOR COMPUTING VIBRATION MODES OF

## THE CARRIER-EXPERIMENT SYSTEM

By William C. Walton, Jr.
Langley Research Center

This appendix explains the method used in the present paper to obtain a mathematical model of a manned carrier vehicle (Skylab) carrying a large telescope (ATM). The math model is a modal model consisting of computed natural vibration modes of structural components. The method has been specially devised to use vibration modes previously computed for the carrier vehicle with the ATM experiment package considered as a rigid attached mass and vibration modes for the ATM considered as an elastic body attached to a rigid base. Special features of the application of the method to the coupled carrier—experiment-package structure are given.

The following assumptions are made:

(1) Computed vibration modes and natural frequencies are available for the carrier structure with the experiment package included as a rigid body attached to the carrier through locked gimbals. These modes will henceforth be referred to as carrier modes.

(2) Computed vibration modes and natural frequencies are available for the experiment package considered as an elastic body gimbaled to a fixed base. These modes will henceforth be referred to as ATM modes.

(3) Lumped-mass analyses were used in obtaining both carrier and ATM modes, and the computed mode shapes are expressed as deflections and rotations at the mass points (see ref. 4, ch. 5, for treatment of vibrations of lumped-mass systems).

(4) The masses and mass-point locations utilized in the computation of the ATM modes are available.

(5) Information necessary to define the connection between the carrier and ATM package is available.

The Lagrangian for the coupled system may now be developed. The vector $\{DC\}$ is defined as the deformation vector used in the calculation of the carrier modes. It is assumed that

$$\{DC\} = [UC]\{QC\} \tag{A1}$$

where the columns of $[UC]$ are carrier modes and $\{QC\}$ is the vector of carrier mode coordinates. The matrix $[UC]$ is generally rectangular. The vector $\{DT\}$ is defined as the deformation vector used in the calculation of ATM modes. It is assumed that

$$\{DT\} = [CONN]\{DC\} + [UT]\{QT\} \tag{A2}$$

where the columns of $[UT]$ are ATM modes, $\{QT\}$ is a vector of ATM mode coordinates, and $[CONN]$ is a matrix to be developed subsequently such that the term $[CONN]\{DC\}$ represents the motion of the ATM package as if it were rigidly attached to the carrier.

The modal analyses which produce carrier modes and ATM modes are based on structural idealizations which are presumed to imply stiffness and mass matrices. Although some of these matrices are not needed in computation, their use is convenient in derivations and they are defined here for that purpose.

Let

$$\{EDT\} = [UT]\{QT\} \tag{A3}$$

Then, the Lagrangian for the coupled system may be written as

$$L = \frac{1}{2}\lfloor DC \rfloor [KC]\{DC\} + \frac{1}{2}\lfloor EDT \rfloor [KT]\{EDT\} - \frac{1}{2}\lfloor \dot{D}C \rfloor \left[\overline{MC}\right]\{\dot{D}C\} - \frac{1}{2}\lfloor \dot{D}T \rfloor [MT]\{\dot{D}T\} \tag{A4}$$

Matrices $[KC]$ and $[MC]$ are, respectively, the symmetric stiffness and mass matrices used to compute carrier modes; $[KT]$ and $[MT]$ are, respectively, the symmetric stiffness and mass matrices used to compute ATM modes; and $\left[\overline{MC}\right]$ is the carrier mass matrix $[MC]$ with the ATM mass deleted.

By referring to equation (A2), equation (A4) may be rewritten as

$$\begin{aligned} L = \frac{1}{2}\Bigg(&-\lfloor \dot{D}C \rfloor\left[\overline{MC}\right]\{\dot{D}C\} - \lfloor \dot{D}C \rfloor[CONN]^T[MT][CONN]\{\dot{D}C\} \\ &-\lfloor \dot{D}C \rfloor[CONN]^T[MT]\{\dot{E}\dot{D}T\} - \lfloor \dot{E}\dot{D}T \rfloor[MT][CONN]\{\dot{D}C\} \\ &-\lfloor \dot{E}\dot{D}T \rfloor[MT]\{\dot{E}\dot{D}T\} + \lfloor DC \rfloor[KC]\{DC\} + \lfloor EDT \rfloor[KT]\{EDT\}\Bigg) \end{aligned} \tag{A5}$$

The second term within the parentheses on the right-hand side of equation (A5) represents the kinetic energy of a motion of the ATM as if the ATM were rigidly attached to the carrier. Therefore, by considering the previously given definition of $\left[\overline{MC}\right]$, the first two

terms within the parentheses may be combined to give

$$L = \frac{1}{2}\Big( \lfloor DC \rfloor [KC]\{DC\} + \lfloor EDT \rfloor [KT]\{EDT\}$$

$$- \lfloor \dot{D}C \rfloor [MC]\{\dot{D}C\} - \lfloor \dot{D}C \rfloor [CONN]^T[MT]\{\dot{E}DT\}$$

$$- \lfloor \dot{E}DT \rfloor [MT][CONN]\{\dot{D}C\} - \lfloor \dot{E}DT \rfloor [MT]\{\dot{E}DT\} \Big) \tag{A6}$$

By using equations (A1) and (A3), equation (A6) can be written as

$$L = \frac{1}{2}\Big( \lfloor QC \rfloor [UC]^T[KC][UC]\{QC\} + \lfloor QT \rfloor [UT]^T[KT][UT]\{QT\}$$

$$- \lfloor \dot{Q}C \rfloor [UC]^T[MC][UC]\{\dot{Q}C\} - \lfloor \dot{Q}C \rfloor [UC]^T[CONN]^T[MT][UT]\{\dot{Q}T\}$$

$$- \lfloor \dot{Q}T \rfloor [UT]^T[MT]^T[CONN][UC]\{\dot{Q}C\} - \lfloor \dot{Q}T \rfloor [UT]^T[MT][UT]\{\dot{Q}T\} \Big) \tag{A7}$$

It is now noted that certain of the expressions which occur in equation (A7) may be written as follows:

$$[UC]^T[MC][UC] = \lceil GMC \rfloor \tag{A8a}$$

$$[UT]^T[MT][UT] = \lceil GMT \rfloor \tag{A8b}$$

$$[UC]^T[KC][UC] = \lceil GMC \rfloor \lceil WSQC \rfloor \tag{A8c}$$

$$[UT]^T[KT][UT] = \lceil GMT \rfloor \lceil WSQT \rfloor \tag{A8d}$$

where $\lceil GMC \rfloor$, $\lceil GMT \rfloor$, $\lceil WSQC \rfloor$, and $\lceil WSQT \rfloor$ are diagonal. The diagonal elements of $\lceil GMC \rfloor$ and $\lceil GMT \rfloor$ are the generalized masses associated with the carrier modes and the ATM modes, respectively. The diagonal elements of $\lceil WSQC \rfloor$ and $\lceil WSQT \rfloor$ are the squares of the natural frequencies associated with the respective modes. The coupling matrix $[CUP]$ is defined by the equation

$$[CUP] = [UC]^T [CONN][MT][UT] \tag{A9}$$

By using equations (A3), (A8), and (A9) in equation (A7), the Lagrangian becomes

$$
L = \frac{1}{2}\lfloor QC \mid QT \rfloor
\begin{bmatrix}
\lceil GMC \rfloor \lceil WSQC \rfloor & 0 \\
\hline
0 & \lceil GMT \rfloor \lceil WSQT \rfloor
\end{bmatrix}
\begin{Bmatrix} QC \\ \hline QT \end{Bmatrix}
$$

$$
- \frac{1}{2}\lfloor \dot{Q}C \mid \dot{Q}T \rfloor
\begin{bmatrix}
\lceil GMC \rfloor & [CUP] \\
\hline
[CUP]^T & \lceil GMT \rfloor
\end{bmatrix}
\begin{Bmatrix} \dot{Q}C \\ \hline \dot{Q}T \end{Bmatrix}
\tag{A10}
$$

Equation (A10) leads to the eigenvalue-eigenvector problem

$$
\left(
\begin{bmatrix}
\lceil GMC \rfloor \lceil WSQC \rfloor & 0 \\
\hline
0 & \lceil GMT \rfloor \lceil WSQT \rfloor
\end{bmatrix}
- \omega_n^2
\begin{bmatrix}
\lceil GMC \rfloor & [CUP] \\
\hline
[CUP]^T & \lceil GMT \rfloor
\end{bmatrix}
\right)
\begin{Bmatrix} UQC \\ \hline UQT \end{Bmatrix} = 0
\tag{A11}
$$

The eigenvalues $\omega_n^2$ of equation (A11) determine the natural frequencies of the coupled carrier-experiment system and the associated eigenvectors $\begin{bmatrix} UQC \mid UQT \end{bmatrix}^T$ are the mode shapes in terms of modal coordinates. To express the mode shapes in terms of physical displacements and rotations, the following equation derived from equations (A1) and (A2) may be used:

$$
\begin{Bmatrix} DC \\ \hline DT \end{Bmatrix} =
\begin{bmatrix}
[UC] & 0 \\
\hline
[CONN][UC] & [UT]
\end{bmatrix}
\begin{Bmatrix} UQC \\ \hline UQT \end{Bmatrix}
\tag{A12}
$$

The model matrix $[U]$ for the coupled carrier-experiment system which is referred to in the text is thus calculated from the equation

$$[U] = \begin{bmatrix} [UC] & 0 \\ \hline [CONN][UC] & [UT] \end{bmatrix} \begin{bmatrix} UQC \\ \hline UQT \end{bmatrix} \tag{A13}$$

where the columns of the matrix on the far right constitute a complete set of eigenvectors of equation (A11).

The matrix $[CONN]$ is derived on the assumption that the ATM package and the carrier vehicle are connected at only one point and that the common point is a mass point of the carrier and also a mass point of the ATM experiment package. Thus, the equation of constraint for locked gimbals can be expressed as

$$\{DRAPT\} = [TAP]\{DRAPC\} \tag{A14}$$

where the elements of the vectors $\{DRAPT\}$ and $\{DRAPC\}$ are deflections and rotations of the attachment point referred to the ATM coordinate system and to the carrier coordinate system, respectively, and where $[TAP]$ is a $6 \times 6$ transformation matrix depending only on the relative orientations of the two coordinate systems. Since the attachment point coincides with mass points of both the ATM and the carrier, the elements of $\{DRAPT\}$ are six consecutive elements of the vector $\{DT\}$, and the elements of $\{DRAPC\}$ are six consecutive elements of $\{DC\}$. If it is assumed that the ATM is rigid, then the vector $\{DT\}$ is related to the attachment-point displacements and rotations by an equation of the form

$$\{DT\} = [ECC]\{DRAPT\}$$

$$= [ECC][TAP]\{DRAPC\} \tag{A15}$$

The matrix $[ECC]$ depends only on the coordinates of the mass points of the ATM referred to the ATM coordinate system. Thus, the matrix $[CONN]$ has the form

$$CONN = \begin{bmatrix} 0 & [ECC][TAP] & 0 \end{bmatrix} \tag{A16}$$

where the finite columns correspond to the six elements in $\{DC\}$ which are identical to the elements of $\{DRAPC\}$.

# APPENDIX B

## FORMULATION OF SYSTEM-TRANSFER-FUNCTION EQUATIONS

### Modal Equations

The basic uncoupled modal differential equations for the composite model are given by equation (1) as

$$\{\ddot{q}\} + 2(0.01)\left[\omega_n\right]\{\dot{q}\} + \left[\omega_n^2\right]\{q\} = [UF]^T\{E\}$$

If the Laplace transform of this equation is taken, it becomes

$$\left([I]s^2 + 2(0.01)\left[\omega_n\right]s + \left[\omega_n^2\right]\right)\{Q\} = [UF]^T\{\bar{E}\} \tag{B1}$$

where $[I]$ is the identity matrix, s is the Laplace operator, $\{Q\}$ is the Laplace transform of $\{q\}$, and $\{\bar{E}\}$ is the Laplace transform of $\{E\}$. For simplification, the diagonal matrix $\left[M\right]$ is defined as

$$\left[M\right] = [I]s^2 + 2(0.01)\left[\omega_n\right]s + \left[\omega_n^2\right] \tag{B2}$$

Then,

$$\{Q\} = \left[M\right]^{-1}[UF]^T\{\bar{E}\} \tag{B3}$$

If $\{D\}$ represents the Laplace transform of the modal displacements in carrier coordinates found by transforming equation (2), then

$$\{D\} = [UD]\{Q\} \tag{B4}$$

Finally, substituting from equation (B3) results in

$$\{D\} = [UD]\left[M\right]^{-1}[UF]^T\{\bar{E}\} \tag{B5}$$

## System Transfer Function

A block diagram of the experiment-package $Y_T$- and $Z_T$-axis servo loops and one general set of crew-motion filters is given in figure 3. The crew-motion filters are the blocks labeled $K_7$ through $K_{12}$. First, the transfer-function equations for the crew-motion input, labeled $\bar{F}(s)$, will be developed and then the transfer-function equations for the stability analysis will be developed from these equations. In figure 3, $\epsilon_5$, $\epsilon_6$, $\epsilon_{19}$, and $\epsilon_{20}$ correspond to $\{D\}$ in equation (B5) and $\epsilon_3$, $\epsilon_4$, $\epsilon_9$, $\epsilon_{10}$, and $\epsilon_{13}$ through $\epsilon_{18}$ correspond to $\{\bar{E}\}$ in the same equation. With reference to figure 3, the matrix equation that includes each $\epsilon$ $\left(\text{with } \theta_{cy} \text{ and } \theta_{cz} \text{ set to zero and with input } \bar{F}(s)\right)$ is

$$
\begin{Bmatrix}
\epsilon_2 \\ \epsilon_8 \\ \epsilon_3 \\ \epsilon_4 \\ \epsilon_9 \\ \epsilon_{10} \\ \epsilon_{13} \\ \epsilon_{14} \\ \epsilon_{15} \\ \epsilon_{16} \\ \epsilon_{17} \\ \epsilon_{18} \\ \epsilon_5 \\ \epsilon_{11} \\ \epsilon_{19} \\ \epsilon_6 \\ \epsilon_{20} \\ \epsilon_{12}
\end{Bmatrix}
=
\left[
\begin{array}{ccccccccccccccc}
0 & 0 & 0 & -H_1 & 0 & 0 & -K_1 & 0 & 0 & 0\,0\,0\,0\,0\,0\,0\,0\,0\,0\,0\,0\,0\,0\,0 \\
0 & 0 & 0 & 0 & -H_2 & 0 & 0 & 0 & -K_4 & 0\,0\,0\,0\,0\,0\,0\,0\,0\,0\,0\,0\,0\,0\,0 \\
0 & K_2 & 0 & & & & & & & \\
0 & K_3 & & & & & & & & \\
0 & 0 & K_5 & & & & & & & \\
0 & 0 & K_6 & & & & & & & \\
K_7 & 0 & 0 & & & & 0 & & & \\
K_8 & 0 & 0 & & & & & & & \\
K_9 & 0 & 0 & & & & & & & \\
K_{10} & 0 & 0 & & & & & & & \\
K_{11} & 0 & 0 & & & & & & & \\
K_{12} & 0 & 0 & & & & & & & \\
0 & 0 & 0 & 0 & 0 & s & 0 & 0 & 0 & 0\,0\,0\,0\,0\,0\,0\,0\,0\,0\,0\,0\,0\,0\,0 \\
0 & 0 & 0 & 0 & 0 & 0 & 0 & s & 0 & 0\,0\,0\,0\,0\,0\,0\,0\,0\,0\,0\,0\,0\,0\,0 \\
0 & 0 & 0 & 0 & 0 & 0 & 0 & 0 & 0 & \\
0 & 0 & 0 & 0 & 0 & 0 & 0 & 0 & 0 & [UD]\left[M\right]^{-1}[UF]^T \\
0 & 0 & 0 & 0 & 0 & 0 & 0 & 0 & 0 & \\
0 & 0 & 0 & 0 & 0 & 0 & 0 & 0 & 0 &
\end{array}
\right]
\begin{Bmatrix}
\bar{F}(s) \\ \epsilon_2 \\ \epsilon_8 \\ \epsilon_5 \\ \epsilon_{11} \\ \epsilon_{19} \\ \epsilon_6 \\ \epsilon_{20} \\ \epsilon_{12} \\ \epsilon_3 \\ \epsilon_3 \\ \epsilon_4 \\ \epsilon_4 \\ \epsilon_9 \\ -\epsilon_9 \\ \epsilon_{10} \\ -\epsilon_{10} \\ \epsilon_{13} \\ \epsilon_{14} \\ \epsilon_{15} \\ \epsilon_{16} \\ \epsilon_{17} \\ \epsilon_{18}
\end{Bmatrix}
\qquad \text{(B6)}
$$

Note that in figure 3 each torque motor has two outputs. These outputs represent a torque input into the experiment package and a reaction torque input into the carrier. Since the experiment-package roll ring is considered attached to the carrier in a rigid plane (see appendix A), the reaction torques for one axis go into one location in the carrier. Dividing through the matrix equation (B6) by $\bar{F}(s)$, and then rearranging, results in

$$
\begin{bmatrix}
1 & 0 & 0 & 0 & 0 & 0 & 0 & 0 & 0 & 0 & 0 & 0 & 0 & 0 & 0 & 0 & H_1 & 0 & 0 & K_1 & 0 & 0 \\
0 & 1 & 0 & 0 & 0 & 0 & 0 & 0 & 0 & 0 & 0 & 0 & 0 & 0 & 0 & 0 & 0 & H_2 & 0 & 0 & 0 & K_4 \\
-K_2 & 0 & 1 & & & & & & & & & & & & & & & & & & & \\
-K_2 & 0 & 0 & 1 & & & & & & & & & & & & & & & & & & \\
-K_3 & 0 & 0 & 0 & 1 & & & & & & & & & & & & & & & & & \\
-K_3 & 0 & 0 & 0 & 0 & 1 & & & & & & & & & & & & & & & & \\
0 & -K_5 & 0 & 0 & 0 & 0 & 1 & & & & & & & & & & & & & & & \\
0 & K_5 & 0 & 0 & 0 & 0 & 0 & 1 & & & & & & 0 & & & & & & & & \\
0 & -K_6 & 0 & 0 & 0 & 0 & 0 & 0 & 1 & & & & & & & & & & & & & \\
0 & K_6 & 0 & 0 & 0 & 0 & 0 & 0 & 0 & 1 & & & & & & & & & & & & \\
 & & & & & & & & & & 1 & & & & & & & & & & & \\
 & & & & & & & & & & & 1 & & & & & & & & & & \\
 & & & & 0 & & & & & & & & 1 & & & & & & & & & \\
 & & & & & & & & & & & & & 1 & & & & & & & & \\
 & & & & & & & & & & & & & & 1 & & & & & & & \\
 & & & & & & & & & & & & & & & 1 & & & & & & \\
0 & 0 & 0 & 0 & 0 & 0 & 0 & 0 & 0 & 0 & 0 & 0 & 0 & 0 & 0 & 0 & 1 & 0 & -s & 0 & 0 & 0 \\
0 & 0 & 0 & 0 & 0 & 0 & 0 & 0 & 0 & 0 & 0 & 0 & 0 & 0 & 0 & 0 & 0 & 1 & 0 & 0 & -s & 0 \\
0 & 0 & & & & & & & & & & & & & & & 0 & 0 & 1 & 0 & 0 & 0 \\
0 & 0 & & & & -[UD]\!\left[M\right]^{-1}[UF]^T & & & & & & & & & & & 0 & 0 & 0 & 1 & 0 & 0 \\
0 & 0 & & & & & & & & & & & & & & & 0 & 0 & 0 & 0 & 1 & 0 \\
0 & 0 & & & & & & & & & & & & & & & 0 & 0 & 0 & 0 & 0 & 1
\end{bmatrix}
\begin{Bmatrix}
\hat{T}_2 \\ \hat{T}_8 \\ \hat{T}_3 \\ \hat{T}_3 \\ \hat{T}_4 \\ \hat{T}_4 \\ \hat{T}_9 \\ -\hat{T}_9 \\ \hat{T}_{10} \\ -\hat{T}_{10} \\ \hat{T}_{13} \\ \hat{T}_{14} \\ \hat{T}_{15} \\ \hat{T}_{16} \\ \hat{T}_{17} \\ \hat{T}_{18} \\ \hat{T}_5 \\ \hat{T}_{11} \\ \hat{T}_{19} \\ \hat{T}_6 \\ \hat{T}_{20} \\ \hat{T}_{12}
\end{Bmatrix}
=
\begin{Bmatrix}
0 \\ 0 \\ 0 \\ 0 \\ 0 \\ 0 \\ 0 \\ 0 \\ 0 \\ 0 \\ K_7 \\ K_8 \\ K_9 \\ K_{10} \\ K_{11} \\ K_{12} \\ 0 \\ 0 \\ 0 \\ 0 \\ 0 \\ 0
\end{Bmatrix}
\qquad \text{(B7)}
$$

where a given element in $\{\hat{T}\}$ represents a transfer function with $\bar{F}(s)$ as the input $\left(\text{for example, } \hat{T}_2 = \dfrac{\epsilon_2}{\bar{F}(s)}\right)$. Equation (B7) has the form

$$[A]\{\hat{T}\} = \{B\}$$

The solution for $\{\hat{T}\}$ for a given value of $s$ then is

$$\{\hat{T}\} = [A]^{-1}\{B\} \tag{B8}$$

and $\hat{T}_6$, $\hat{T}_{12}$, $\hat{T}_5$, and $\hat{T}_{11}$ represent, respectively, the transfer function between the crew-motion input and the angle about the $Y_T$-axis at the fine-sun-sensor location, the angle about the $Z_T$-axis at the fine-sun-sensor location, the rate about the $Y_T$-axis at the rate-gyro location, and the rate about the $Z_T$-axis at the rate-gyro location. The equations for these four functions are used in finding the time response. The method for finding the response is presented in appendix C.

By changing the crew-motion input equations slightly, the experiment-package $Y_T$-axis sun-sensor open-loop transfer function and $Z_T$-axis sun-sensor open-loop transfer function can be found. To find the $Y_T$-axis sun-sensor open-loop transfer function, set $\theta_{cy}$ and $\overline{F}(s)$ to zero and change the equation for $\epsilon_2$ as follows:

$$\epsilon_2 = \theta_{cy}K_1 - \epsilon_5 H_1$$

Dividing by $\theta_{cy}$ and transposing gives

$$\hat{T}_2 + \hat{T}_5 H_1 = K_1$$

With this change, equation (B7) can be suitably modified. The $Z_T$-axis sun-sensor open-loop transfer function can be similarly obtained.

# APPENDIX C

## OBTAINING LINEAR-SYSTEM RESPONSE BY USING

## THE DISCRETE FOURIER TRANSFORM

A linear system can be represented as

$$\bar{H}(s) = \bar{R}(s)/\bar{F}(s)$$

f(t) → [ System transfer function ] → r(t)

Random signal input — Pointing error output
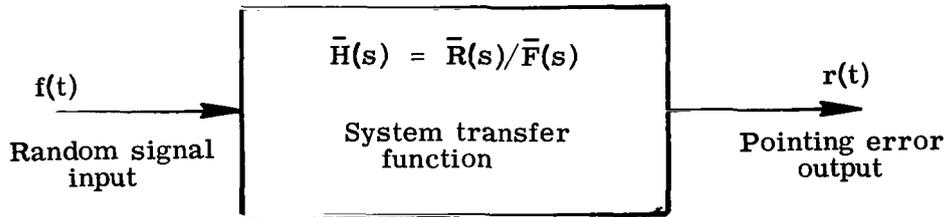
The input  f(t)  to the system and the transfer function  $\bar{H}(s)$  of the system are assumed to be known.  This appendix explains how to obtain the output  r(t)  of the system by using discrete Fourier transform techniques.

### Continuous and Discrete Fourier Transforms

If  f(t)  is defined for a period  $0 \leqq t \leqq T$  and is zero elsewhere, the continuous Fourier transform  $F(\omega)$  can be obtained as

$$F(\omega) = \int_{-\infty}^{\infty} f(t) e^{-i\omega t} \, dt \tag{C1}$$

That is,

$$F(\omega) = \int_{0}^{T} f(t) e^{-i\omega t} \, dt \tag{C2}$$

The transform  $F(\omega)$  can be obtained for any frequency from  $-\infty$  to  $\infty$  and then the time function  f(t)  can be obtained as

$$f(t) = \frac{1}{2\pi} \int_{-\infty}^{\infty} F(\omega) e^{i\omega t} \, d\omega \tag{C3}$$

Now, if  $F(\omega)$  is obtained only for the frequency range  $-\omega_f \leqq \omega \leqq \omega_f$  and if  $\omega_f$  is sufficiently high to make  $F(\omega)$  practically zero for all  $|\omega| > |\omega_f|$, then it is possible to write

$$f(t) = \frac{1}{2\pi} \int_{-\omega_f}^{\omega_f} F(\omega)e^{i\omega t} \, d\omega \qquad \text{(C4)}$$

The two functions $f(t)$ and $F(\omega)$ can be considered as a CFT pair and may be denoted by the symbol $f(t) \longleftrightarrow F(\omega)$.

The system output $r(t)$ can be obtained by convolving the impulse response $h(t)$ with the input $f(t)$. Therefore, if $r(t) \longleftrightarrow R(\omega)$ and $h(t) \longleftrightarrow H(\omega)$, then

$$R(\omega) = H(\omega)F(\omega) \qquad \text{(C5)}$$

and

$$r(t) = \frac{1}{2\pi} \int_{-\infty}^{\infty} H(\omega)F(\omega)e^{i\omega t} \, d\omega \qquad \text{(C6)}$$

If $H(\omega)$ and $F(\omega)$ are available for $-\omega_f \leq \omega \leq \omega_f$, then

$$r(t) = \frac{1}{2\pi} \int_{-\omega_f}^{\omega_f} H(\omega)F(\omega)e^{i\omega t} \, d\omega \qquad \text{(C7)}$$

It can be seen that $H(\omega)$ can be obtained from the transfer function $\bar{H}(s)$ of the system by replacing $s$ by $i\omega$; that is,

$$H(\omega) = \bar{H}(i\omega) \qquad \text{(C8)}$$

Thus, if the input $f(t)$ and the transfer function $\bar{H}(s)$ are known, it is possible to obtain the output $r(t)$.

However, if the system is to be analyzed on a digital computer, one must use the finite, discrete version of the Fourier transform (that is, the discrete Fourier transform (DFT)), and all the functions or the waveforms have to be sampled and cannot be continuous.

If the input $f(t)$ is defined for $0 \leq t \leq T$ and sampled at a uniform interval of time $\Delta t$, an array $f(k)$, with $k = 1,2,\ldots,N$, will be obtained defining the function $f(t)$. Now, analogous to the CFT pair, a DFT pair $f(k) \longleftrightarrow F(j)$ can be defined as

$$F(j) = \frac{1}{N} \sum_{k=1}^{N} f(k)e^{\frac{-2\pi i(k-1)(j-1)}{N}} \qquad (j = 1,2,\ldots,N) \qquad \text{(C9)}$$

and

$$f(k) = \sum_{j=1}^{N} F(j) e^{\frac{-2\pi i (k-1)(j-1)}{N}} \qquad (k = 1,2,\ldots,N) \qquad (C10)$$

where $f(k)$ and $F(j)$ are, in general, complex sequences defining functions in the time domain and frequency domain, respectively.

It can be seen that time and frequency are not explicit in equations (C9) and (C10). However, the index $k$ refers to a sample period number and the index $j$ represents a harmonic number. The true time and frequency corresponding to these indices can be obtained as

$$t_k = (k - 1)\Delta t \qquad (C11)$$

and

$$f_j = (j - 1)\Delta f \qquad (C12)$$

where

$$\Delta f = f_0 = \frac{1}{T} \qquad (C13)$$

At this stage, it should also be noted that the sequences $f(k)$ and $F(j)$ are periodic over $N$ because of the exponential term in equations (C9) and (C10). As explained subsequently, this property of the DFT has important implications when two time sequences are convolved.

Now, if $f(t)$ is a real time function, the sequence $f(k)$ is real and the sequence $F(j)$ has the following properties (see fig. 5):

(1) The real part of $F(j)$ is symmetric about $f_f = \frac{N}{2} f_0$, called the "folding frequency"; that is,

$$\mathrm{Re}\ F(j) = \mathrm{Re}\ F(N + 2 - j) \qquad \left(j = 2,3,\ldots,\frac{N}{2}\right) \qquad (C14)$$

(2) The imaginary part of $F(j)$ is antisymmetric about the folding frequency $f_f$; that is,

$$\mathrm{Im}\ F(j) = -\mathrm{Im}\ F(N + 2 - j) \qquad \left(j = 2,3,\ldots,\frac{N}{2}\right) \qquad (C15)$$

27

The two numbers $F(1)$ and $F\left(\frac{N}{2} + 1\right)$ in the array $F(j)$ correspond to zero and folding frequency, respectively.

Now, since the sequence $F(j)$ is periodic, one can say that the real part of $F(j)$ is an even function and that the imaginary part of $F(j)$ is an odd function. In other words, the Fourier coefficients $F\left(\frac{N}{2} + 2\right), \ldots, F(N)$ can be viewed as the negative frequency harmonics for frequencies between $-\left(f_f - f_o\right)$ and $-f_o$.

### Periodic and Aperiodic Convolutions Using the DFT

When the functions in the time domain are sampled, the convolution of two sequences $f_1(k)$ and $f_2(k)$, which in the frequency domain is represented by the product of their DFT's, takes the following form:

$$F_1(j)F_2(j) \longrightarrow \frac{1}{N} \sum_{n=1}^{N} f_1(n)f_2(j - n + 1) = \frac{1}{N} \sum_{n=1}^{N} f_1(j - n + 1)f_2(n) \qquad (j = 1, 2, \ldots, N) \qquad (C16)$$

As pointed out earlier, the sequences $f_1(k)$, $f_2(k)$, $F_1(j)$, and $F_2(j)$ are periodic over $N$; that is, if $f(k) \longrightarrow F(j)$, then $F(j)$ is a periodic function over a frequency band $0$ to $f_s$ and describes the DFT of a time function $f(k)$ which is periodic over a period $0$ to $T$. As a result, the convolution defined by equation (C16) is also periodic.

Now, if the input $f(t)$ which is sampled over $0$ to $T$ is periodic over $T$, then the steady-state output $r(t)$ for a linear system will also be periodic over $T$ and the convolution defined in equation (C16) will correctly describe the recurrent transients of $r(t)$. However, the use of equation (C16) when $f(t)$ is not periodic over $T$ will be incorrect and the sequences have to be suitably modified.

To illustrate the unwanted periodicity in convolution, assume two sequences $f_1(k)$ and $f_2(k)$ as shown in figure 6. The N-point convolution $f_3(k)$ of these two sequences can be written as

$$f_3(k) = \frac{1}{N} \sum_{n=1}^{N} f_1(n)f_2(k - n + 1) = \frac{1}{N} \sum_{n=1}^{N} f_1(k - n + 1)f_2(n) \qquad (k = 1, 2, \ldots, N) \qquad (C17)$$

This computation corresponds to reversing one sequence and sliding it past the other in increments as the summing operation of equation (C17) is performed. Let $f_2(k)$ be fixed. Figure 7 shows the sequence $f_1(k)$ reversed in time and positioned for computation of the first point $f_3(1)$. The first two points can be written as

$$f_3(1) = \frac{1}{N}\Big[f_1(1)f_2(1) + f_1(0)f_2(2) + f_1(-1)f_2(3)$$
$$+ f_1(-2)f_2(4) + f_1(-3)f_2(5) + f_1(-4)f_2(6)\Big] \qquad (C18)$$

and

$$f_3(2) = \frac{1}{N}\Big[f_1(2)f_2(1) + f_1(1)f_2(2) + f_1(0)f_2(3)$$
$$+ f_1(-1)f_2(4) + f_1(-2)f_2(5) + f_1(-3)f_2(6)\Big] \qquad (C19)$$

Notice that the negative indices can be interpreted by the following equation because of periodicity of the sequences

$$f_1(-j) = f_1(N - j) \qquad (j = 0,1,2,. . .,(N-2)) \qquad (C20)$$

As each point of the reversed sequence $f_1(k)$ is shifted out to the right, the corresponding point is shifted in on the left; hence, unless the sequence being shifted is periodic over N, the convolution performed by equation (C17) will be erroneous. This situation can be easily remedied and an aperiodic convolution can be obtained as follows. If two sequences are described by N points, N more points having zero value can be added to the sequence to make a total of 2N elements in the sequence. The DFT, the inverse DFT, and hence the convolution will then be periodic over 2N, and an N-point convolution of the two sequences defined in this manner will give an aperiodic convolution of two N-point sequences. This method is illustrated in figures 8 and 9 and described in detail in reference 9.

### Computation of the Sampled Output

A step-by-step procedure has been described below to obtain the system output $r(t)$ when the input $f(t)$ and the transfer function $\bar{H}(s)$ are known:

(1) Choose a value for N such that the folding frequency $f_f = \frac{N}{2T}$ is high enough to describe the transfer function adequately.

(2) Sample the input $f(t)$ over T at a uniform interval of time $\left(\Delta t = \frac{T}{N}\right)$ and obtain the sequence $f(k)$, with $k = 1,2,. . .,N$. Extend the sequence by adding zero terms to a total of 2N terms. Thus, an array $f(k)$, with $k = 1,2,. . .,2N$, is obtained such that

$$f(k) = f\left[(k - 1)\Delta t\right] \qquad\qquad (k = 1,2,\ldots,N)$$

$$f(k) = 0 \qquad\qquad (k = (N+1),(N+2),\ldots,2N)$$

(3) Operate the DFT of $f(k)$ and obtain the sequence $F(j)$, with $j = 1,2,\ldots,2N$. The increment in frequency corresponding to the two consecutive values of $F(j)$ is then $f_O = \dfrac{1}{2T}$.

(4) Define the sequence $H(m)$ as follows:

$$H(m) = \bar{H}\left[i2\pi(m - 1)f_O\right] \qquad\qquad (m = 1,2,\ldots,(N+1))$$

$$H(N + 1 + j) = \text{conj } H(N + 1 - j) \qquad\qquad (j = 1,2,\ldots,(N-1))$$

(5) Obtain the array

$$R(m) = H(m)F(m) \qquad\qquad (m = 1,2,\ldots,2N)$$

(6) Operate the inverse DFT on $R(m)$.

(7) Form the array $r(m)$ such that

$$r(m) = \text{Re } R(m) \qquad\qquad (m = 1,2,\ldots,N)$$

The array $r(m)$ defines the sampled output $r(t)$ over the period $0 \leqq t \leqq T$.

# REFERENCES

1. George C. Marshall Space Flight Center:  Scientific Experiments for the Apollo Telescope Mount.  NASA TN D-5020, 1969.

2. Chubb, W. B.; and Seltzer, S. M.:  Skylab Attitude and Pointing Control System.  NASA TN D-6068, 1971.

3. Smith, P. G.:  The Pointing Accuracy of an Orbiting Gimbal Mounted Telescope.  TM 69-1022-2, Bellcomm, Inc., Feb. 17, 1969.  (Available as NASA CR-106643.)

4. Anderson, Roger A.:  Fundamentals of Vibrations.  Macmillan Co., c.1967.

5. Keckler, Claude R.; Kyle, Robert G.; Will, Ralph W.; and Woolley, Charles T.:  Real-Time Digital-Computer-Hardware Simulation of a Spacecraft With Control-Moment-Gyroscope Stabilization.  NASA TM X-2069, 1970.

6. Smith, P. G.:  A Mathematical Model for Simulation of the Apollo Telescope Mount Pointing Control System.  TR-68-620-1 (Contract NASW-417), Bellcomm, Inc., May 8, 1968.  (Available as NASA CR-95402.)

7. Hendricks, T. C.; and Johnson, C. H.:  Stochastic Crew Motion Modeling.  J. Spacecraft Rockets, vol. 8, no. 2, Feb. 1971, pp. 150-154.

8. Cooley, James W.; and Tukey, John W.:  An Algorithm for the Machine Calculation of Complex Fourier Series.  Math. Comput., vol. 19, no. 90, Apr. 1965, pp. 297-301.

9. Bergland, G. D.:  A Guided Tour of the Fast Fourier Transform.  IEEE Spectrum, vol. 6, no. 7, July 1969, pp. 41-52.

## TABLE I.- NOMINAL PARAMETERS OF THE ATM CONTROL SYSTEM

Fine-sun-sensor gain, $H_s$, volts/rad . . . . . . . . . . . . . . . . . . . . . . . . 33 000

Rate-gyro gain, $K_{rg}$, volts/rad/sec . . . . . . . . . . . . . . . . . . . . . . . 2580

Torque-motor gain, $K_a K_m$, N-m/volt . . . . . . . . . . . . . . . . . . . . . 37.95

Fine-sun-sensor time constant, $\tau_s$, sec . . . . . . . . . . . . . . . . . . . . 0.016

Torque-motor time constant, $\tau_a$, sec . . . . . . . . . . . . . . . . . . . . . 0.0032

Rate-gyro natural frequency, $\omega_g$, rad/sec . . . . . . . . . . . . . . . . . . 154.88

Rate-gyro damping ratio, $\rho_g$ . . . . . . . . . . . . . . . . . . . . . . . . . 0.8

## TABLE II.- CREW-MOTION FILTER PARAMETERS

| Crew motion | Input | Input axis | $\rho_1$ | $\bar{\omega}_1$ | $\rho_2$ (a) | $\bar{\omega}_2$ (a) | $\tau_1$ | $\tau_2$ |
|---|---|---|---|---|---|---|---|---|
| Console operation Run 1 | Force | $X_C$ | 0.5056 | 4.0291 | 0 | 0 | 4.1091 | 0 |
| | | $Y_C$ | .5565 | 2.8065 | 0 | 0 | 3.8489 | 0 |
| | | $Z_C$ | .5986 | 4.7634 | 0.2357 | 31.2563 | 2563.12 | 0 |
| | Moment | $X_C$ | 0.3196 | 4.4158 | 0 | 0 | 7.27 | 0 |
| | | $Y_C$ | .4683 | 4.0384 | 0 | 0 | 12.7861 | 0 |
| | | $Z_C$ | .5589 | 4.4132 | 0 | 0 | 2.9666 | 0 |
| Console operation Run 4 | Force | $X_C$ | 0.6176 | 4.8207 | 0 | 0 | 6.2389 | 0 |
| | | $Y_C$ | .4660 | 3.9640 | 0 | 0 | 5.6195 | 0 |
| | | $Z_C$ | .7719 | 5.3108 | 0 | 0 | 5.6142 | 0 |
| | Moment | $X_C$ | 0.4846 | 4.5882 | 0 | 0 | 13.8367 | 0 |
| | | $Y_C$ | .6750 | 4.3448 | 0 | 0 | 20.7737 | 0 |
| | | $Z_C$ | .7691 | 5.3496 | 0 | 0 | 5.9213 | 0 |
| Compressive walking | Force | $X_C$ | 0.2097 | 4.7567 | 0 | 0 | 1.2428 | 0 |
| | | $Y_C$ | .2601 | 14.0260 | 0.3831 | 2.9387 | 375.92 | 0.07 |
| | | $Z_C$ | .4509 | 8.0629 | 0 | 0 | 7.2673 | 0 |
| | Moment | $X_C$ | 0.2509 | 1.2705 | 0.1231 | 13.3204 | 931.01 | 0 |
| | | $Y_C$ | .3839 | 4.0364 | .3196 | 16.9327 | 2106.51 | 0 |
| | | $Z_C$ | .3386 | 2.7191 | .1850 | 13.0889 | 476.43 | 0 |

[a] If $\rho_2$ and $\bar{\omega}_2$ are zero, then the term $\left(s^2 + 2\rho_2\bar{\omega}_2 s + \bar{\omega}_2{}^2\right)$ is deleted from equation (3).

## TABLE III.- PARAMETERS FOR COMPUTATION OF
## ERROR TIME HISTORIES

Number of points in sequences $f(k)$, $r(m)$, etc., $N$ . . . . . . . . . . . . . . . . . . 2048

Folding frequency, $f_f$, rad/sec . . . . . . . . . . . . . . . . . . . . . . . . 300

Sampling interval in time domain, $\Delta t$, sec . . . . . . . . . . . . . . . . . . . . 0.01047

Period of $f(t)$, $T$, sec . . . . . . . . . . . . . . . . . . . . . . . . . . . 21.45


## TABLE IV.- RIGID-BODY $3\sigma$ POINTING ERRORS FOR
## FINE-SUN-SENSOR LOCATION

| Crew motion | Carrier location | $3\sigma$ errors, arc sec | |
| --- | --- | --- | --- |
| | | $\theta_{ey}$ | $\theta_{ez}$ |
| Console Operation Run 1 | AM/MDA intersection | $0.3935 \times 10^{-3}$ | $0.4160 \times 10^{-3}$ |
| Console Operation Run 4 | AM/MDA intersection | .6273 | .6560 |
| Compressive walking | AM/MDA intersection | .9888 | 1.0423 |
| Compressive walking | OWS crew location | .5289 | .5824 |

## TABLE V.- RIGID-ATM $3\sigma$ POINTING ERRORS FOR FINE-SUN-SENSOR LOCATION

| Crew motion | Carrier location | $3\sigma$ errors, arc sec | |
| --- | --- | --- | --- |
| | | $\theta_{ey}$ | $\theta_{ez}$ |
| Console Operation Run 1 | AM/MDA intersection | $3.8494 \times 10^{-3}$ | $4.2426 \times 10^{-3}$ |
| Console Operation Run 4 | AM/MDA intersection | 5.3867 | 5.8878 |
| Compressive walking | AM/MDA intersection | 7.4736 | 7.8396 |
| Compressive walking | OWS location | 2.5270 | 2.6880 |

## TABLE VI.- FLEXIBLE-BODY $3\sigma$ POINTING ERRORS FOR FINE-SUN-SENSOR LOCATION

| Crew motion | Carrier location | $3\sigma$ errors, arc sec | |
| --- | --- | --- | --- |
| | | $\theta_{ey}$ | $\theta_{ez}$ |
| Console Operation Run 1 | AM/MDA intersection | $9.766 \times 10^{-3}$ | $12.672 \times 10^{-3}$ |
| Console Operation Run 4 | AM/MDA intersection | 11.971 | 15.860 |
| Compressive walking | AM/MDA intersection | 15.500 | 20.130 |
| Compressive walking | OWS crew location | 2.996 | 3.218 |

$Y_C$

$X_C$

CSM

$Z_T$

$Y_T$

OWS

$Z_T$ — ATM canister

$X_T$

LM

c.m. (-3.627, -.023, -1.524)

$X_C$

MDA

$Z_C$

AM/MDA crew location
(-3.81, 0, 0)

OWS crew location
(-16.92, 0, 3.05)
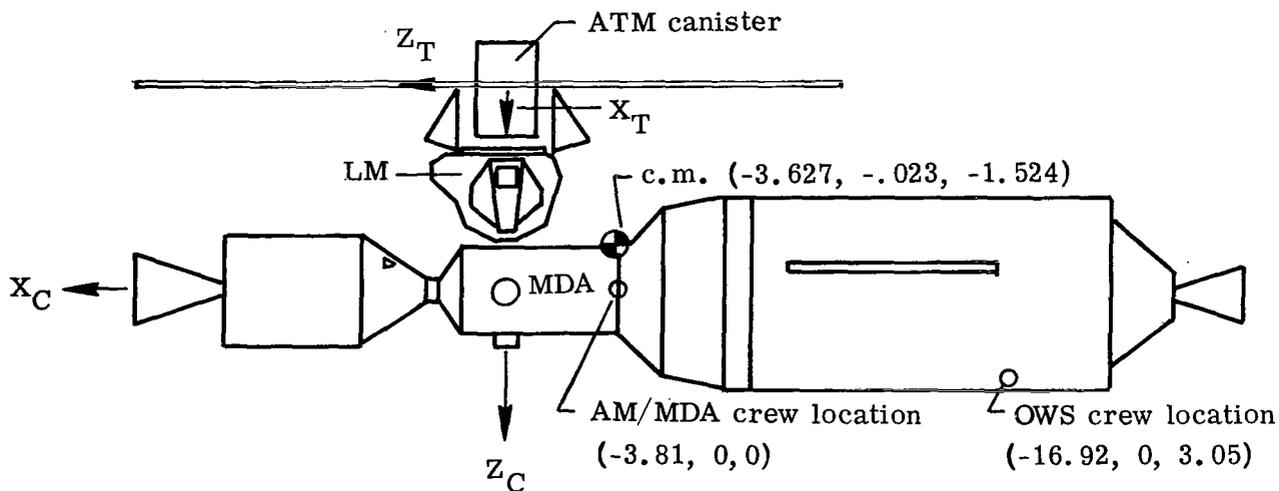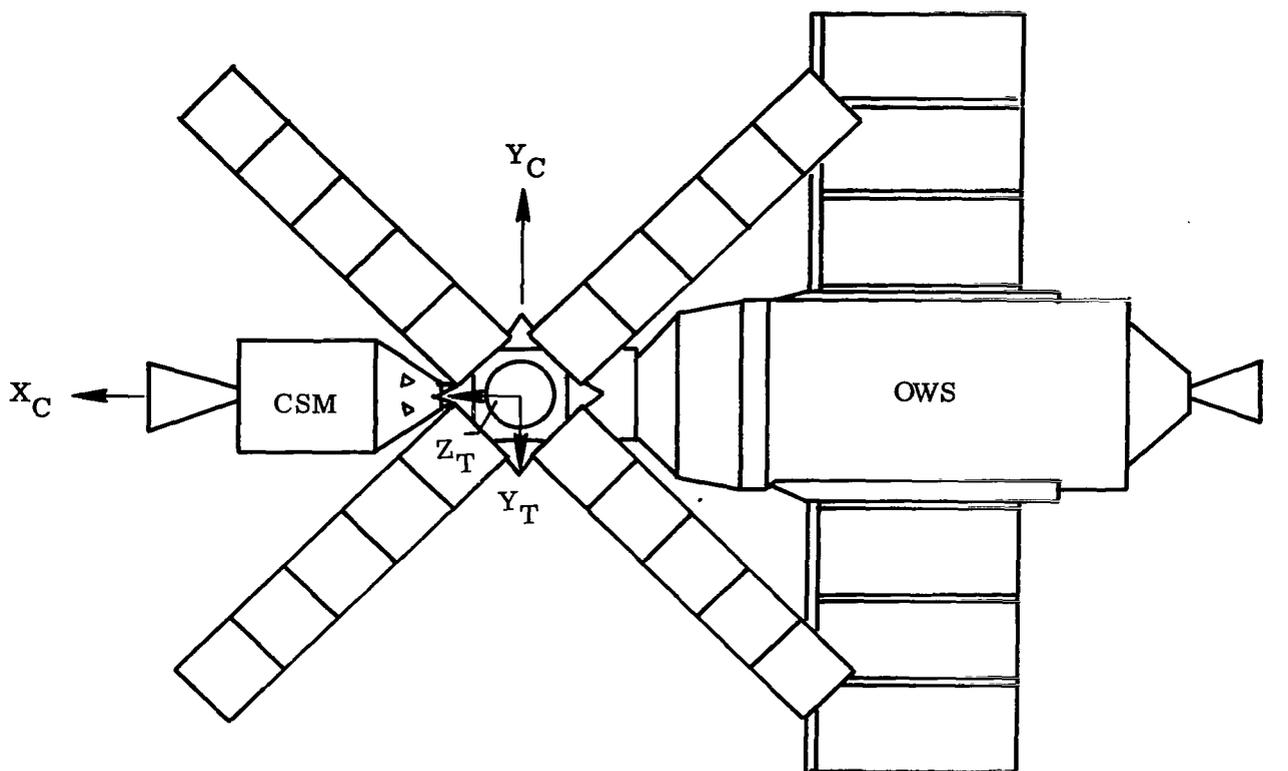
Figure 1.- Skylab configuration. (Locations are given in meters.)
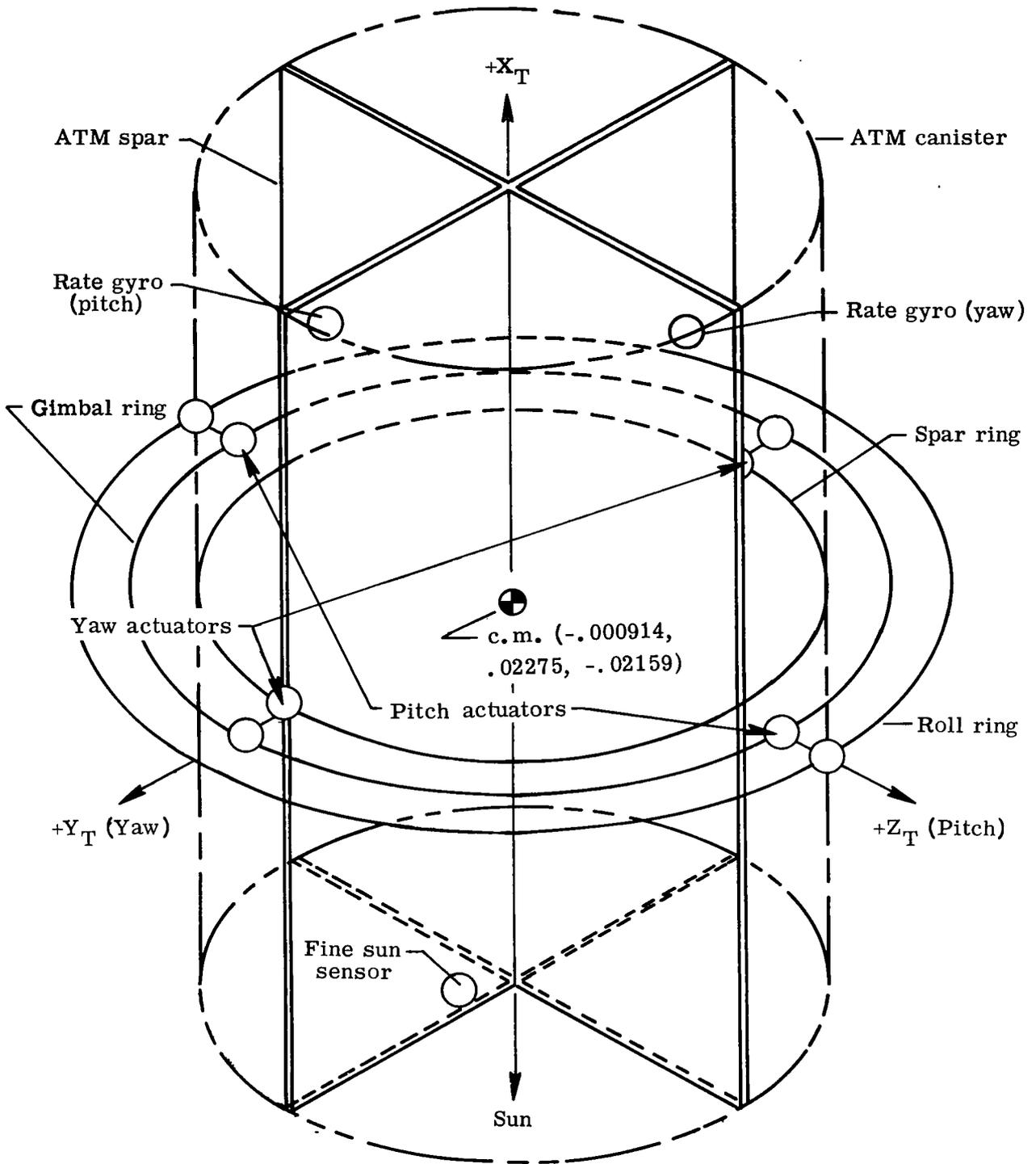
(a) Spar and ring assembly.  (Center-of-mass location is given in meters.)

Figure 2.- ATM configuration.

Sun

Gimbal ring

Torque
motors

ATM
experiment
package

$Y_T$ (yaw)

$X_T$ (roll)

Roll ring

$Z_T$ (pitch)
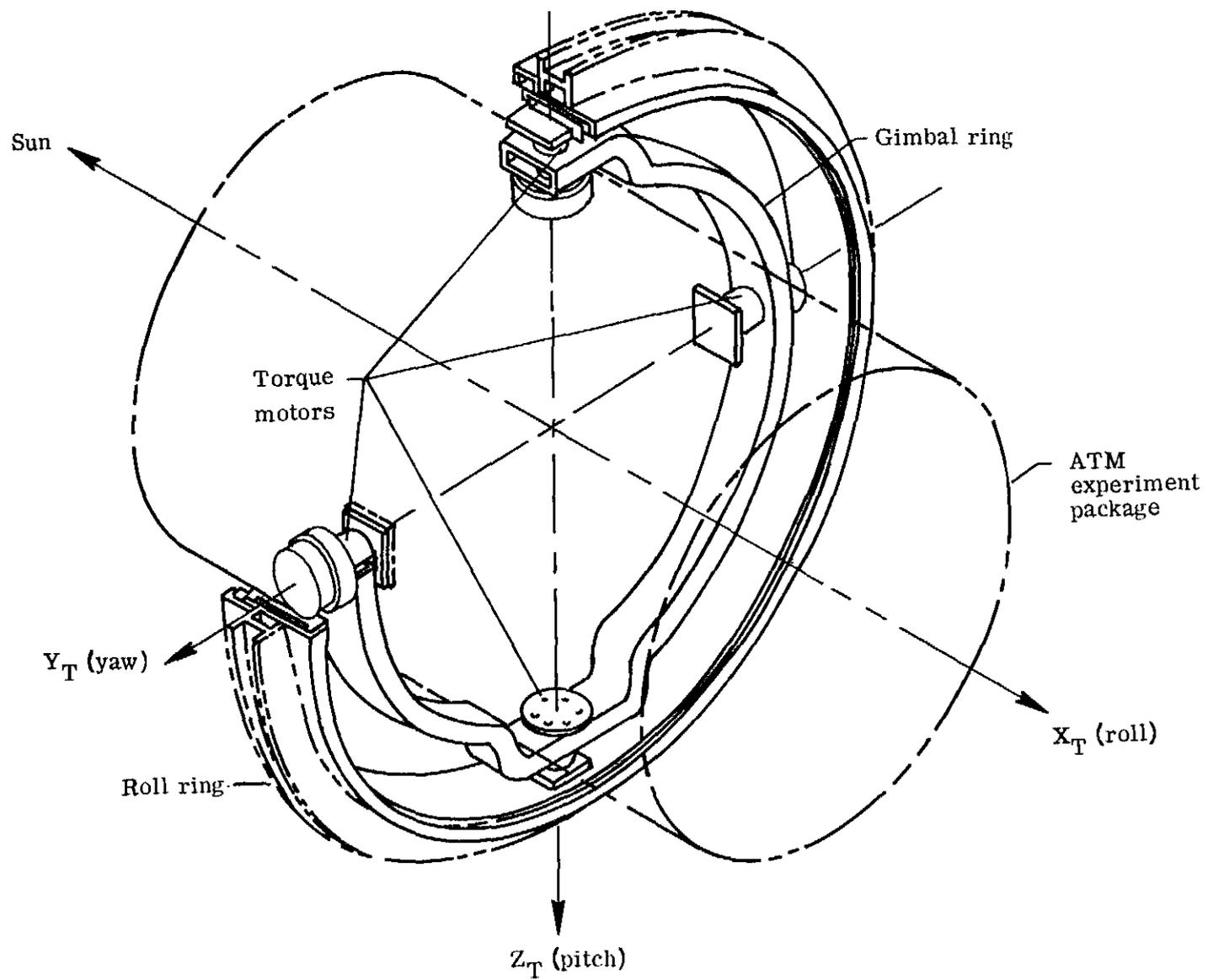
(b) Gimbal system.

Figure 2.- Concluded.
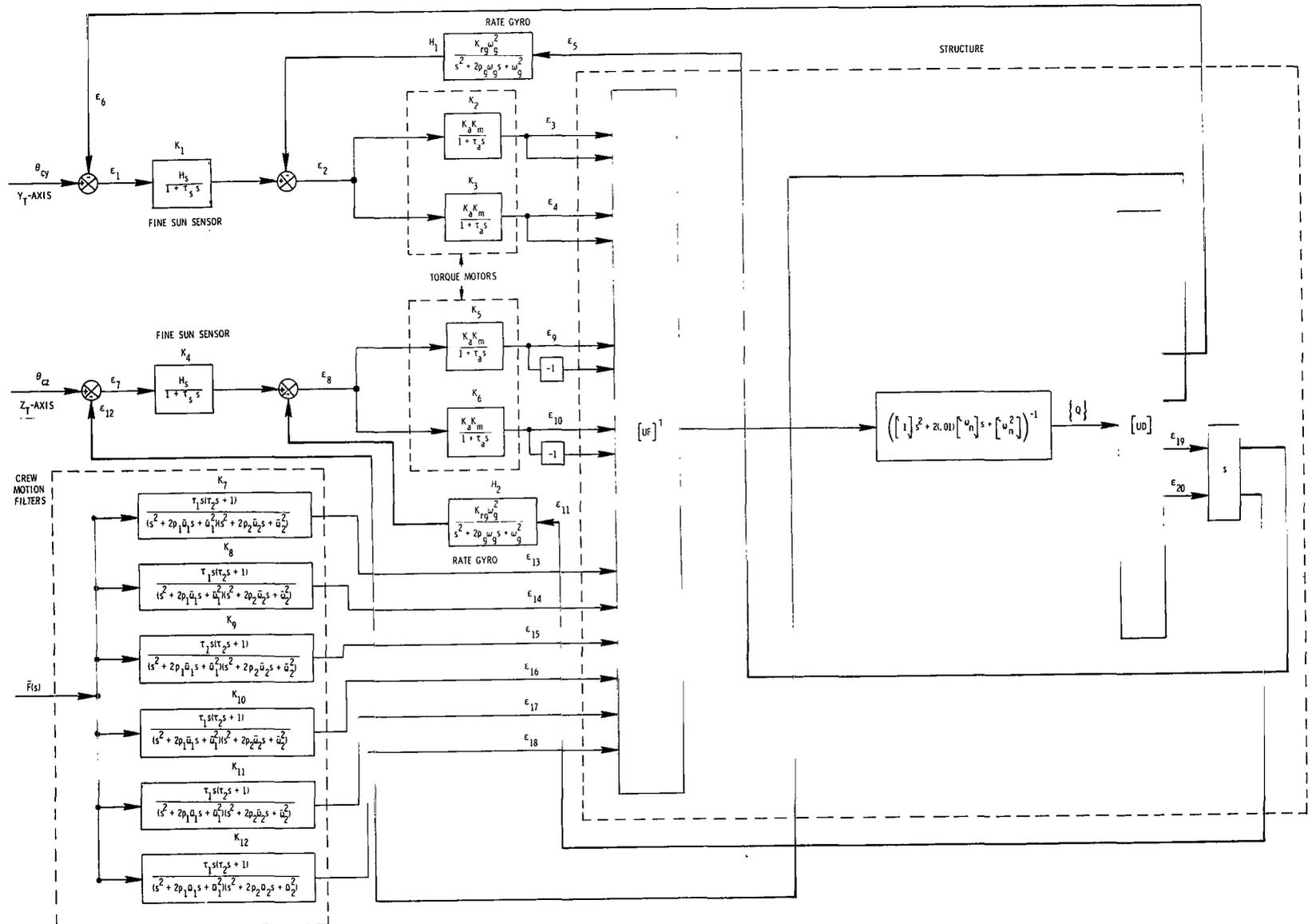
Figure 3.- System block diagram.
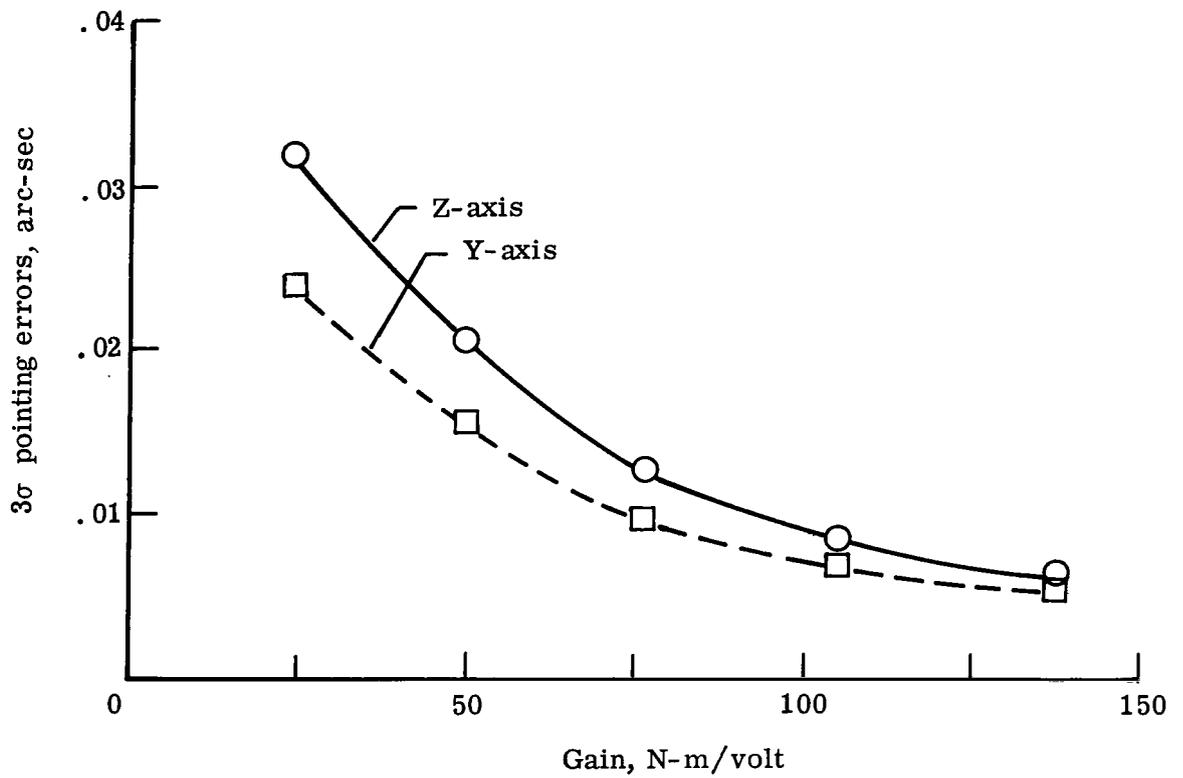
Figure 4.- Variation of total 3σ pointing errors with torque-motor gain for fine-sun-sensor location.
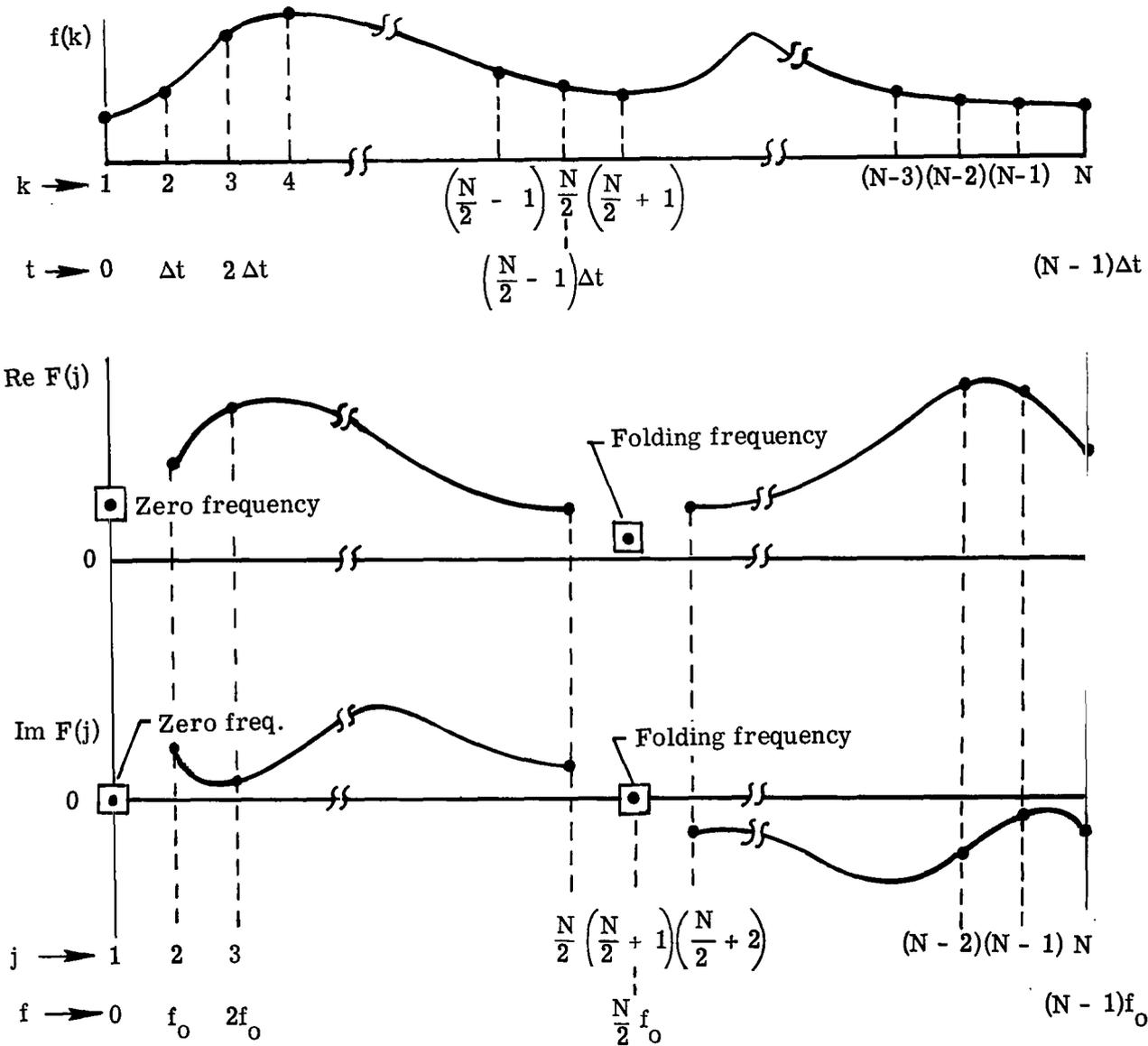
Figure 5.- Format of the discrete Fourier transform of a real time function.
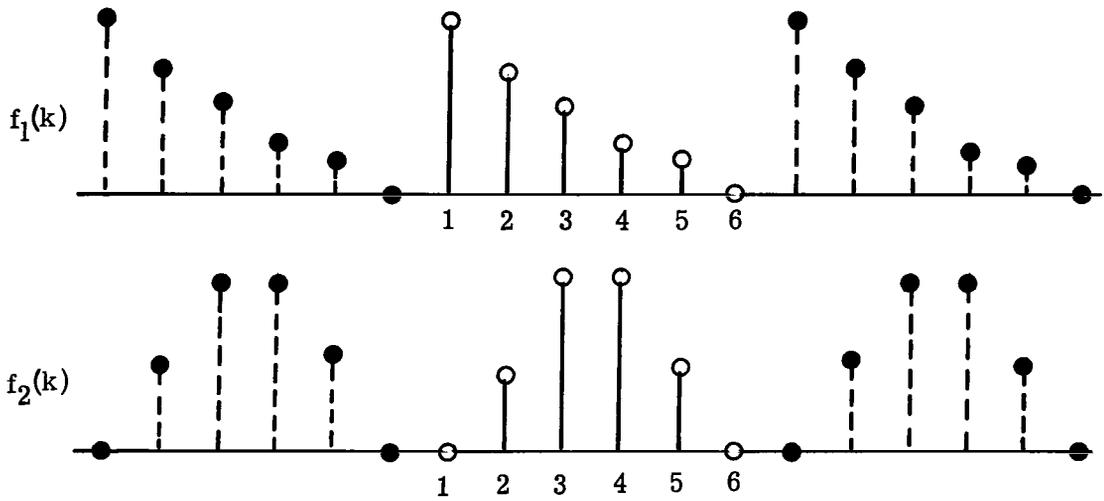
Figure 6.- Sequences $f_1(k)$ and $f_2(k)$.
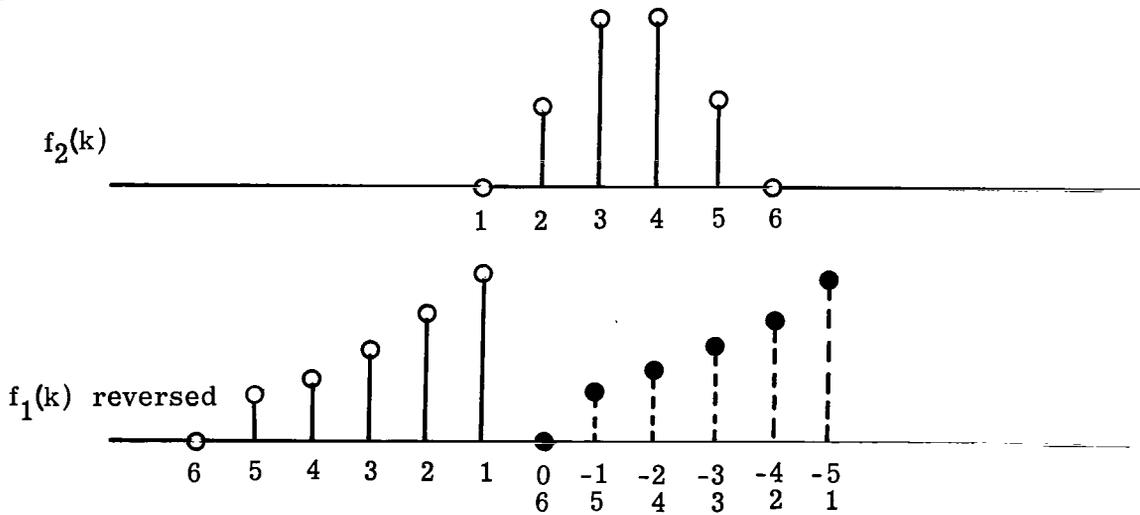


Figure 7.- Sequence $f_2(k)$ fixed and sequence $f_1(k)$ reversed in
time for convolution.
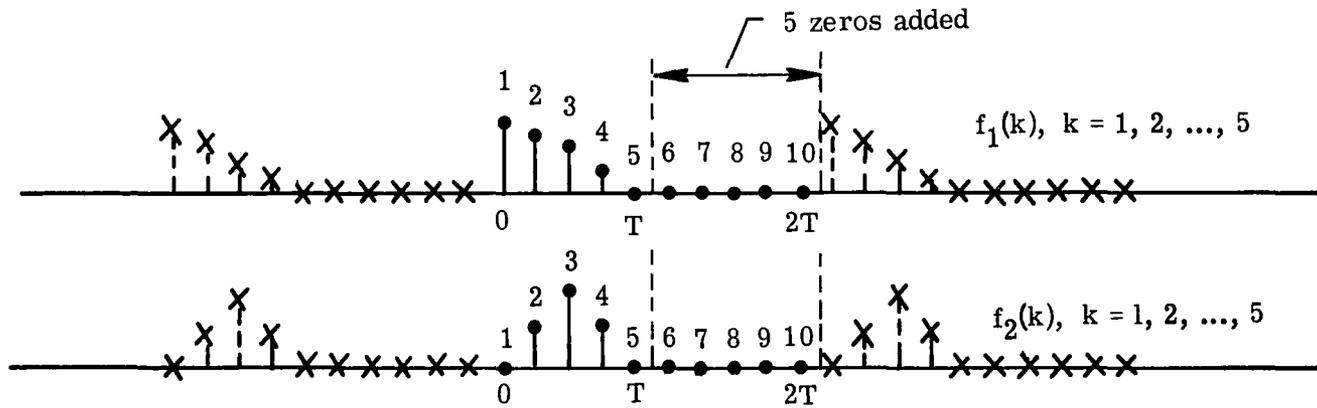
Figure 8.- Sequences $f_1(k)$ and $f_2(k)$ with $N$ zeros added.
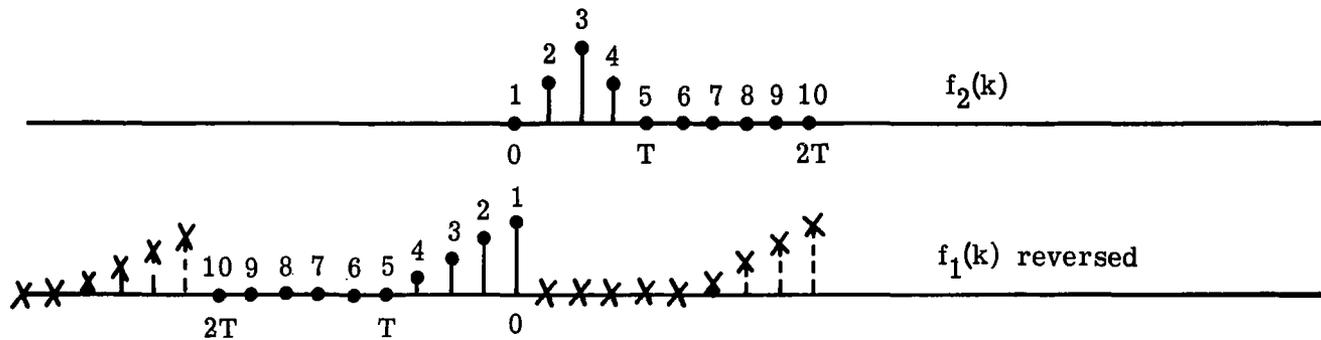


Figure 9.- Sequences $f_1(k)$ and $f_2(k)$ in position for computation of an N-point aperiodic convolution.

*"The aeronautical and space activities of the United States shall be conducted so as to contribute . . . to the expansion of human knowledge of phenomena in the atmosphere and space. The Administration shall provide for the widest practicable and appropriate dissemination of information concerning its activities and the results thereof."*

— NATIONAL AERONAUTICS AND SPACE ACT OF 1958

# NASA SCIENTIFIC AND TECHNICAL PUBLICATIONS

**TECHNICAL REPORTS:** Scientific and technical information considered important, complete, and a lasting contribution to existing knowledge.

**TECHNICAL NOTES:** Information less broad in scope but nevertheless of importance as a contribution to existing knowledge.

**TECHNICAL MEMORANDUMS:** Information receiving limited distribution because of preliminary data, security classification, or other reasons.

**CONTRACTOR REPORTS:** Scientific and technical information generated under a NASA contract or grant and considered an important contribution to existing knowledge.

**TECHNICAL TRANSLATIONS:** Information published in a foreign language considered to merit NASA distribution in English.

**SPECIAL PUBLICATIONS:** Information derived from or of value to NASA activities. Publications include conference proceedings, monographs, data compilations, handbooks, sourcebooks, and special bibliographies.

**TECHNOLOGY UTILIZATION PUBLICATIONS:** Information on technology used by NASA that may be of particular interest in commercial and other non-aerospace applications. Publications include Tech Briefs, Technology Utilization Reports and Technology Surveys.

*Details on the availability of these publications may be obtained from:*

## SCIENTIFIC AND TECHNICAL INFORMATION OFFICE

# NATIONAL AERONAUTICS AND SPACE ADMINISTRATION
### Washington, D.C. 20546